Characterization of the KATRIN cryogenic pumping section

C. Röttele [a,1], M. Steidl [b], M. Sturm [a,*], M. Röllig [a], A. Marsteller [a], L. Schimpf [c,d,1], F. Friedel [b,1], A. Jansen [b], W. Gil [b], M. Schrank [b], J. Wolf [c], G. Drexlin [c], B. Bornschein [a]

[a] Institute for Astroparticle Physics Tritium, Laboratory Karlsruhe(IAP-TLK), Karlsruhe Institute of Technology (KIT), Hermann-von-Helmholtz-Platz 1, 76344 Eggenstein-Leopoldshafen, Germany
[b] Institute for Astroparticle Physics (IAP), Karlsruhe Institute of Technology (KIT), Hermann-von-Helmholtz-Platz 1, 76344 Eggenstein-Leopoldshafen, Germany
[c] Institute of Experimental Particle Physics (ETP), Karlsruhe Institute of Technology (KIT), Wolfgang-Gaede-Str. 1, 76131 Karlsruhe, Germany
[d] Institut für Kernphysik, Westfälische Wilhelms-Universität Münster, Wilhelm-Klemm-Str. 9, 48149 Münster, Germany

A R T I C L E   I N F O

A B S T R A C T

The KArlsruhe TRItium Neutrino (KATRIN) experiment aims to determine the effective anti-electron neutrino mass with a sensitivity of $0.2\,eV/c^2$ by using the kinematics of tritium β-decay. It is crucial to have a high signal rate which is achieved by a windowless gaseous tritium source producing 10^{11} β-electrons per second. These are guided adiabatically to the spectrometer section where their energy is analyzed. In order to maintain a low background rate below $0.01\,cps$, one essential criteria is to permanently reduce the flow of neutral tritium molecules between the source and the spectrometer section by at least 14 orders of magnitude. A differential pumping section downstream from the source reduces the tritium flow by seven orders of magnitude, while at least another factor of 10^7 is achieved by the cryogenic pumping section where tritium molecules are adsorbed on an approximately $3\,K$ cold argon frost layer. In this paper, the results of the cryogenic pumping section commissioning measurements using deuterium are discussed. The cryogenic pumping section surpasses the requirement for the flow reduction of 10^7 by more than one order of magnitude. These results verify the predictions of previously published simulations.

1. Introduction

The KArlsruhe TRItium Neutrino (KATRIN) experiment uses tritium β-decay in order to analyze the effective electron anti-neutrino mass with a design sensitivity of $0.2\,eV/c^2$ (90 % C.L.) [1]. The result of the first KATRIN tritium measurement campaign improved the upper limit to $1.1\,eV/c^2$ (90 % Confidence Level) [2].

The full KATRIN beam line is illustrated in Fig. 1. In the spectrometer section, the energy of electrons from tritium decay in the source are analyzed by a Magnetic Adiabatic Collimation combined with an Electrostatic filter (MAC-E filter [3]), providing a sharp energy cutoff with a resolution of approximately $\Delta E = 2.8\,eV$ at $E = 18.6\,keV$ depending on the magnetic field setting [2]. The spectrometer section comprises two spectrometers; the pre-spectrometer filters out all low energetic β-electrons while the main spectrometer is used for the energy analysis. The focal plane detector (FPD) terminates the KATRIN beam line and counts all electrons with kinetic energies exceeding the main spectrometer potential.

In order to reach the designed KATRIN sensitivity, a low background rate on the $10\,mcps^2$-level is essential [1]. One important background component, which has to be removed, is caused by neutral tritium molecules (HT, DT, T_2) entering the spectrometer section. If tritium decays there, the resulting β-electron could overcome the retarding potential of the spectrometer. However, due to the high magnetic field at both ends of the spectrometer and the four orders of magnitude lower field in the center, an electron with an energy of up to $18.6\,keV$ would be trapped between the two strong magnets [4]. Subsequently, it would slowly dissipate its energy through scattering, ionizing residual gas molecules (pressure in the $1 \times 10^{-11}\,mbar$ range) in the process. The multitude of low-energy secondary electrons following a single tritium decay in the spectrometer would be accelerated in the electric field of the MAC-E filter. Most of them could reach energies close to the retarding potential, which would render them indistinguishable from signal electrons.

Consequently, the transport and pumping section was designed to provide a reduction factor of at least 10^{14} for neutral tritium. Tritium

---

* Corresponding author.
  E-mail address: michael.sturm@kit.edu (M. Sturm).
[1] No longer affiliated.
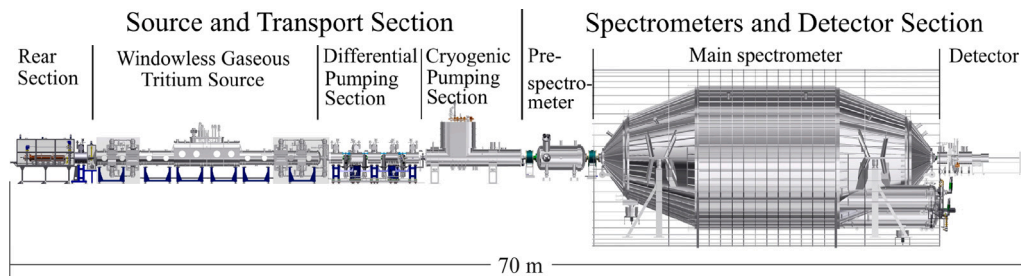[2] Milli counts per second

Fig. 1. The 70-m-long KATRIN beamline is shown with its different components.

is injected at the center of the Windowless Gaseous Tritium Source (WGTS), which is kept at a constant temperature, with a constant flow rate, leading to a stable gas density inside the source and thereby a stable source activity. At both ends of the WGTS, the tritium gas is constantly pumped out in a dedicated gas processing system, non-hydrogen impurities are removed from the gas stream and the cleaned tritium gas is returned to a pressure controlled buffer vessel and re-injected in the WGTS, resulting in a closed circulation loop [5]. At the same time, β-electrons from tritium decays inside the source tube are magnetically guided through the transport and pumping section, composed of the Differential Pumping Section (DPS) and Cryogenic Pumping Section (CPS).

The first stage of reduction is provided by the WGTS and DPS, using turbo-molecular pumps (TMP) to reduce the tritium flow by a factor of 10^7 [6–8]. The cryogenic pumping section is the second and final part of the KATRIN pumping section and has to reduce the incoming neutral tritium flow by at least another factor of 10^7. A section of about 3 m of the CPS beam tube is cooled down to approximately 3 K and covered with an argon frost layer. Incoming tritium molecules are adsorbed on the frosted surface with high efficiency. Before reaching an accumulated activity of 3.7×10^{10} Bq ($\hat{=}1$ Curie), the cryogenic pump is regenerated for safety reasons by replacing the contaminated argon layer with a fresh layer.

In previous publications [9,10], the reduction factor of the CPS has been estimated by simulations. The simulations indicated that the requirements would be met. In the following, the commissioning measurements of the CPS cold trap with deuterium are described and their results discussed in the context of these simulations.

2. Cryogenic pumping section

The CPS is described in detail in Refs. [10,11]. The focus of this section is on the parts most relevant to the context of this paper.

In Fig. 2, the CPS magnet cryostat is shown with its major components. It consists of seven consecutive beam tube sections, where sections 2–5 form the cold trap, which is prepared with an argon frost layer. Beam tube sections 2–4 build a chicane increasing the probability for neutral gas to hit the cold trap surface. Furthermore, fins are attached in beam tube sections 2–5 to increase the total surface available for tritium adsorption. The surface of all stainless steel beam tube elements is gold-plated, suppressing tritium diffusion into them [12]. Additionally, there are two pump ports; the first one is for the regeneration of the argon frost layer, while the second one is for calibration and monitoring purposes in the KATRIN setup [13,14]. There are two liquid helium vessels, one at 4.5 K, the other at 3 K. In order to cool the cold trap down to 3 K, helium supplied by the 4.5-K vessel is pumped down to a pressure of 0.2 bar in the 3-K vessel. For the argon frost preparation a well defined amount of argon (6.042 bar ℓ) is frozen on the beam tube sections 2-4,[3] corresponding to about 3000

monolayers by a dedicated argon inlet system. During the preparation, the cold trap is warmed up to 6 K to produce argon frost with a high porosity and capacitance [15]. Argon is injected into the beam tube by nine capillaries, three in each beam tube section 2–4. Each capillary has 23 homogeneously distributed orifices allowing for a homogeneous distribution over the whole cold trap. After a maximal accumulated activity of 3.7×10^{10} Bq ($\hat{=}1$ Ci) on the cold trap, corresponding to 60 days of KATRIN operation, the argon frost layer is removed by purging the beam tube with about 250 bar ℓ helium while warming it up to 80 K.

3. Measurements

3.1. Experimental setup

For the reduction factor measurements of the CPS argon frost layer a dedicated gas inlet system was installed in front of the CPS (see Fig. 3) [16]. In order to have similar conditions to nominal tritium operation, the injection flow has to be in the molecular flow regime. An adjustable leak-valve was used to vary the flow of deuterium gas in the range between 10^{-3} to 10^{-7} mbar ℓ/s. For the determination of the injection flow, the calibrated conductance of an orifice (diameter of 0.5 mm) and a pressure sensor between the leak-valve and the orifice were used [16]. Before each measurement, a 15.86 ℓ buffer vessel, which was installed in front of the leak-valve, was filled with approximately 200 mbar deuterium to provide sufficient fore-line pressure.

3.2. Measurement procedure

The results of two different measurement procedures are discussed in this paper.

Constant cold trap temperature
For this measurement, a constant deuterium flow was injected into the cold trap with the CPS at its nominal temperature of 3 K. The goal was to test the stability of the deuterium reduction factor along the cold trap over several days. By measuring the pressure p_{PP1} in front of the cold trap with a cold cathode gauge (located at CPS-PP1 in Fig. 3) and p_{PP2} behind the cold trap with a residual gas analyzer (located at CPS-PP2), the CPS reduction factor R_{CPS} can be derived from the pressure ratio

$$R_{\mathrm{CPS}} = \frac{q_{\mathrm{in}}}{q_{\mathrm{out}}} = k \cdot \frac{p_{\mathrm{PP1}}}{p_{\mathrm{PP2}}} \ . \tag{1}$$

The simulated correction factor $k = 18$ [10], relates the measured pressure ratio at the two pump ports to the flow ratio through the upstream flange q_{in} and the downstream flange q_{out} of the CPS beam tube. In the TPMC simulation with MOLFLOW [17] the numbers are related to the density distribution inside the vacuum chamber. Since the vacuum gauges are both at room temperature the density ratio is equal to the measured pressure ratio. Therefore, the pressure ratio can be used for determining the gas flow reduction factor. During the whole measurement, the residual gas analyzer only recorded the partial

---

[3] In beam tube section 5, no argon frost surface is actively prepared.
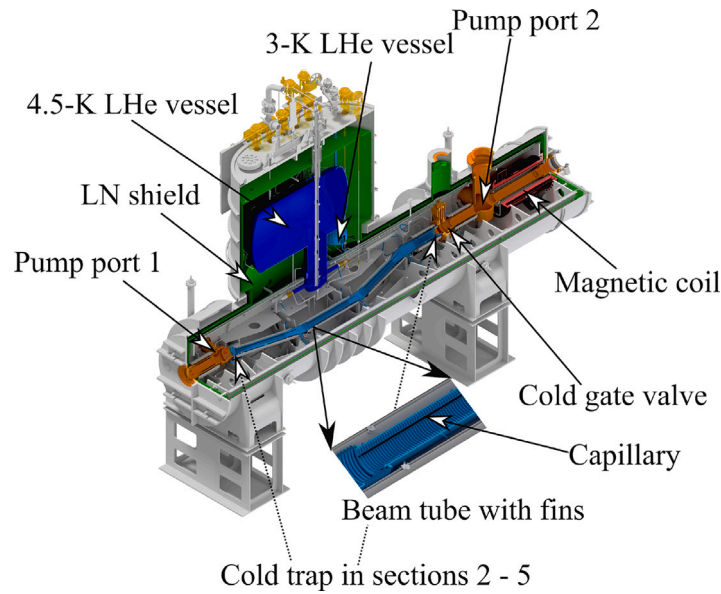
Fig. 2. A CAD drawing of the CPS magnet cryostat is shown in a three-quarter cut. The CPS consists of seven sections; section 2–5 form the cold trap cooled down to approximately 3 K and are highlighted in light blue. At the bottom, a part of the cold trap beam tube is shown zoomed in illustrating the fins and one capillary for the argon injection. For simplification, the magnetic coil is only inserted around the final section in the picture.
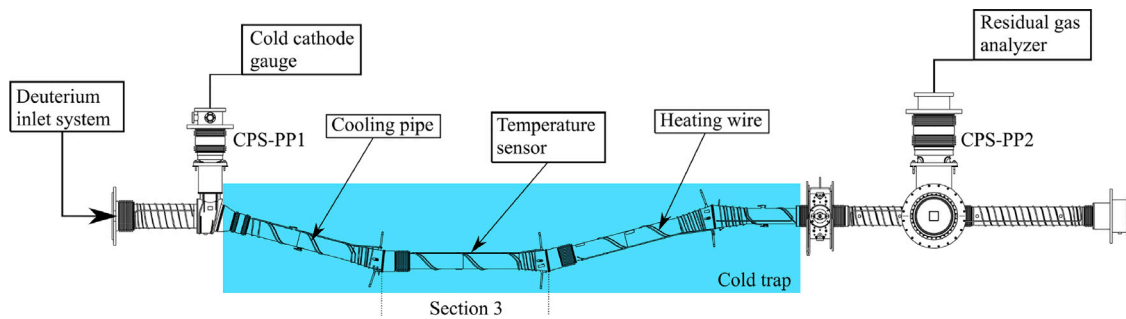
Fig. 3. A simplified measurement setup is shown. The deuterium inlet system is connected to the entrance of the CPS beam tube. During the measurements the valves before and after the CPS (not drawn) are closed. The pressure is recorded at CPS-PP1 (cold cathode gauge of type *MKS 423*) and at CPS-PP2 (residual gas analyzer type *Pfeiffer QMS 200*). The position of the cold trap is highlighted in blue and the temperature sensor (used in the second measurement procedure) is located on the backside of beam tube section 3. The hollow winding around the beam tube represents the cooling pipe which is mounted parallel to the heating wire (filled black winding).

pressure for the mass-to-charge ratio, corresponding to single charged molecules with a mass of 4 amu.

Temperature dependence of cold trap

In the measurement described above, the sensitivity of the RGA connected to CPS-PP2 was not sufficient to measure directly the reduction factor at the nominal operating temperature. Since the reduction factor decreases at higher temperatures of the argon frost, the temperature dependence of the cold trap was investigated in a second measurement. The data were used to extrapolate the observed reduction factors at higher temperatures into the nominal temperature range. During the measurement the temperature of the cold trap was slowly increased, while injecting a constant deuterium flow q_{in}. In order to pass through the entire cold trap, simulations show that a deuterium molecule has to be adsorbed and desorbed more than 2×10^4 times due to the two chicanes and the fins along the beam tubes, assuming smooth stainless steel surfaces. For the real measurement, the rough surface of the argon frost layer is expected to increase the number of hits considerably.

At lower temperatures the time of a molecule through the cold trap of the CPS is dominated by the sojourn time of the adsorption/desorption processes. At increasing temperatures the transmission time is more and more dominated by the time of flight between the surface hits. Due to the large number of surface hits along the cold beam tubes, the temperature dependence of the reduction factor is

expected to follow the temperature dependence of the sojourn time τ_{des} of adsorbed molecules for the investigated temperature range:

$$\tau_{des}(T) = \tau_0 \cdot \exp\left(\frac{E_{des}}{RT}\right) \ . \tag{2}$$

The material and gas specific time constant $\tau_0 \approx 10^{-13}$ s, the desorption enthalpy E_{des}, and the molar gas constant R are independent of the temperature T. This simplified model is used to fit the data and to extrapolate the expected reduction factor to lower temperatures.

4. Results

4.1. Constant cold trap temperature

In the first measurement, a constant flow of 1×10^{-3} mbar ℓ/s was injected at the CPS entrance for 139 h with the cold trap at its nominal temperature. Fig. 4 shows the progression of the pressure of the first reduction measurement. The integrated pV amount at room temperature of the injected deuterium is determined by the pressure between the leak valve and the orifice, multiplied with the conductance of the orifice. The nearly linear increase indicates the constant injection flow of deuterium into the cold trap with only minor variations.

After constant deuterium injection starts at $t_{ini} = 5$ h, the pressure p_{PP1} is elevated from 5×10^{-9} mbar by more than two orders of
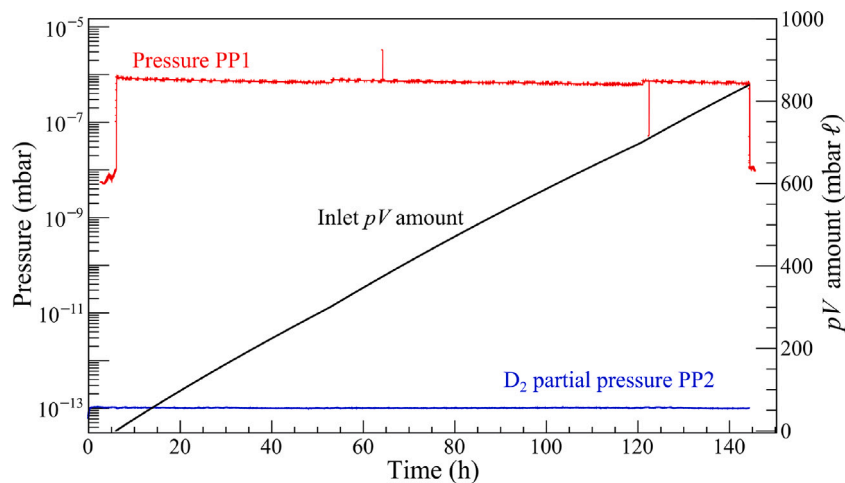
Fig. 4. Reduction factor measurement of CPS — The (partial) pressure at PP1 (red) and PP2 (blue) are plotted over the measurement time. The pressure reading is corrected for deuterium. On the right *y*-axis, the inserted *pV* amount of deuterium is shown and plotted in black.
Source: The figure is adapted from [16].

magnitude within $0.08\,\mathrm{h}$ where it remains until the measurement was stopped at $t_{\mathrm{end}} = 145\,\mathrm{h}$. The two spikes at $63\,\mathrm{h}$ and $122\,\mathrm{h}$ are related to fluctuations in the nitrogen cooling of the CPS radiation shield, which briefly influenced the pressure reading. After around $t_1 = 55\,\mathrm{h}$ and $t_2 = 118\,\mathrm{h}$ the gas flow was slightly adjusted to compensate for the small decrease in the fore-line pressure.

The deuterium partial pressure reading at CPS-PP2 was constant over the whole time, measuring at the sensitivity limit of the residual gas analyzer. With this data a lower limit on the reduction factor can be determined using Eq. (1)

$$
\begin{aligned}
R_{\mathrm{CPS}} &\gtrsim k \cdot \frac{p_{\mathrm{PP1}}(t = 140\,\mathrm{h})}{p_{\mathrm{PP2}}(t = 140\,\mathrm{h})} \\
&\gtrsim 18 \cdot \frac{6.75 \times 10^{-7}\,\mathrm{mbar}}{9.92 \times 10^{-14}\,\mathrm{mbar}} = (1.22 \pm 0.17) \times 10^{8} \ .
\end{aligned}
\tag{3}
$$

The uncertainty is estimated by the error of the cold cathode reading of $\approx 10\%$ [18] and by an independent calibration measurement of the RGA [16].

4.2. Temperature dependence of cold trap

As mentioned in Ref. [10], the cold trap temperature distribution is inhomogeneous. A temperature sensor located in beam tube section 3 (see Fig. 3) is chosen as a reference for the analysis. This sensor reading represents an average temperature due to its position in between the cooling pipe winding which is also confirmed by the results of the COMSOL Multiphysics® cold trap temperature simulation described in Ref. [10]. The measurement is performed by setting temperature values of the cooling pipe and measuring the pressure at PP1 and PP2. After adjusting the temperature of the cooling pipe to a new value, it takes a couple of minutes for the cold trap temperatures to reach equilibrium.

In Fig. 5, the pressure and temperature during the second measurement are shown. During the whole time of about five hours, the injected gas flow was kept at a constant level of $4 \times 10^{-4}\,\mathrm{mbar}\,\ell/\mathrm{s}$. In contrast to Fig. 4, the partial pressure at CPS-PP2 rises when the temperature is above approximately $6\,\mathrm{K}$.

When a new temperature value was set, a correlation with pressure peaks at PP1 can be seen. These peaks are caused by the temperature increase in beam tube section 1 and PP1, which goes hand in hand with the one of the cold trap, leading to an unstable PP1 pressure during the temperature change. For the analysis, only data within a stable temperature period (deviation smaller than $0.15\,\mathrm{K}$ for more than $100\,\mathrm{s}$) is used and therefore the peaks at PP1 are excluded. After the temperature and pressures have stabilized, the average pressure of at

least $100\,\mathrm{s}$ was taken for each gauge to determine the pressure ratio for the corresponding temperature step.

The measurement was stopped after the D_2 partial pressure at PP2 reached $1 \times 10^{-7}\,\mathrm{mbar}$, when it was only one order of magnitude below the inlet pressure. Above $10\,\mathrm{K}$ the pressure ratio does not change significantly anymore, since the system reached the point where the reduction factor is mainly determined by the geometry of the $4.74\,\mathrm{m}$ long beam tube between CPS-PP1 and CPS-PP2 [16].

In Fig. 6, the dependence of the pressure ratio on the cold trap temperature is shown. For the temperature T an uncertainty of $0.12\,\mathrm{K}$[4] is estimated while the pressure uncertainties are equal to those presented for the first measurement procedure. These experimental uncertainties are added in quadrature to the standard deviation of the binned regions. An exponential fit $p_{\mathrm{PP1}}/p_{\mathrm{PP2}} = exp(A + B/T)$ versus T was performed with the best fit parameters $A = -18.3 \pm 0.7$ and $B = 186.7 \pm 5.6\,\mathrm{K}$. From parameter B the molar desorption enthalpy can be derived according to Eq. (2):

$$
E_{\mathrm{des}} \approx (1553 \pm 46)\ \mathrm{J\ mol^{-1}} .
\tag{4}
$$

Here only the statistical uncertainty of the fit is stated.

From the pressure ratio a lower limit for the reduction factor can be extrapolated with Eq. (1). Since the factor $22 > k > 6$ is varying with temperature, time, and the sticking coefficient [10], a conservative lower limit of $k = 6$ is used. The minimum reduction factor $R_{\mathrm{CPS}} = 10^7$ is reached at a temperature of $5.5\,\mathrm{K}$.

5. Discussion

Two different measurement methods with deuterium have been performed to characterize the CPS cold trap prior to tritium operation. These measurements cannot be performed with tritium: the CPS would be operated with several orders of magnitude larger amounts of tritium than the allowed maximum during standard operation. The second measurement method would lead to an unacceptable contamination beyond the cold gate valve and therefore to an intolerable increase in the spectrometer background rate. The major difference between deuterium and tritium is the additional desorption of molecules due to radioactive decays of adsorbed molecules in case of tritium. Its impact is discussed at the end of this section.

Due to the sensitivity limit of the residual gas analyzer and the requirement of molecular injection flow, only a lower limit of the

_____

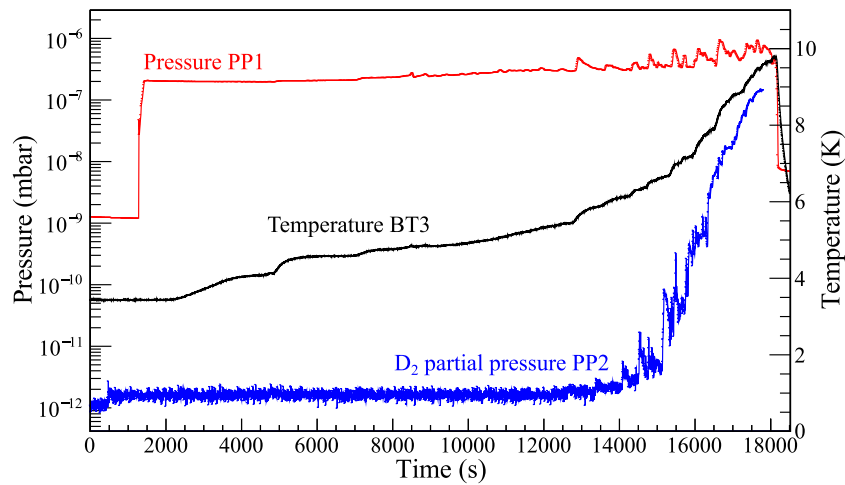[4] This uncertainty is based on an internal KATRIN report.

Fig. 5. The (partial) pressures at both CPS pump ports in mbar are plotted on the left *y*-axis over the measurement time in seconds. Additionally, the temperature of one sensor on beam tube section 3 is shown in black.
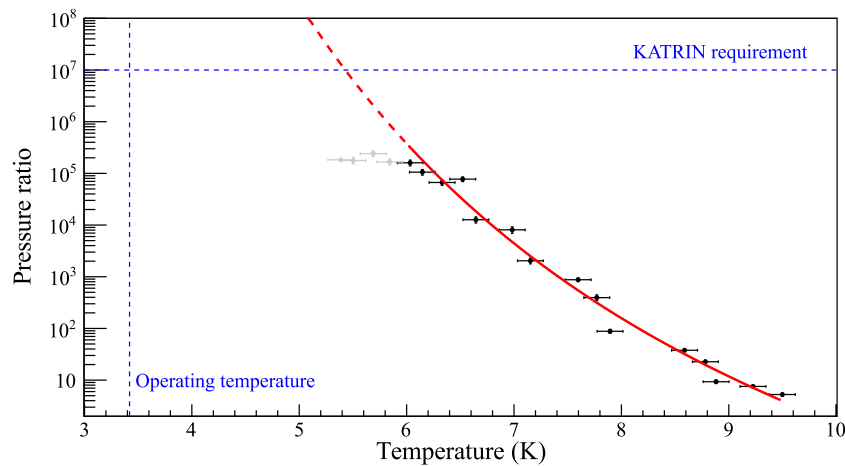*Source:* The figure is adapted from [16].

Fig. 6. The deuterium pressure ratio of both CPS pump ports is plotted over the temperature of a beam tube section 3 sensor. The solid red line shows the fit according to the exponential dependency in Eq. (2). The dashed line extrapolates the fit to lower temperatures. The gray points are excluded from the fit since the RGA was at its sensitivity limit. The horizontal dashed blue line corresponds to the minimum required reduction factor of 10^7 while the vertical one indicates the nominal operation temperature. The figure is adapted from [16]. Using Eq. (1) the reduction factor can be derived from the measured pressure ratio.

reduction factor $R_{\text{CPS}} \geq (1.22 \pm 0.17) \times 10^8$ can be stated by the first measurement method. Nevertheless, the lower limit is already one order of magnitude above the requirement of 10^7. Additionally, the total amount of injected deuterium is more than 100 times the equivalent of the standard 60 days of operation, implying a larger than required capacity of the argon frost layer, which leaves a comfortable safety margin for the operation of the CPS. Therefore, during tritium operation the capacity limit is defined by the radioactive safety limit of 1 Ci rather than the limitations of the cold trap performance.

The second measurement at different cold trap temperatures supports the findings of the first one. A simple extrapolation from the temperature range between 6 and 10 K to the nominal temperature of 3.4 K using the conservative correction factor $k = 6$, yields a reduction factor in the order of 10^{16}. Due to the exponential behavior, the uncertainty of such an extrapolation to the nominal operating temperature is large, surpassing the fit range of the pressure ratio by ten orders of magnitude, which is well above the required 7 orders of magnitude. However, it is not possible to determine an exact central value for the reduction factor with this method, as for increasing temperature steps the time dependent change of previously adsorbed deuterium molecules along the beamline cannot be quantified. Preparing a new argon frost layer for every temperature set point was not possible, as for every new preparation the cold valve at the downstream end of the cold section has to be closed, which has a guarantied life time of only 200 operation cycles. For the result on the desorption energy, several assumptions have been made, which the uncertainties cannot be fully quantified. The most notable one is the usage of one temperature sensor of the cold trap, which can only be seen as an average temperature. Therefore, the stated uncertainty has to be treated carefully. Nevertheless, the measurement performed at a constant temperature also indicates a large desorption energy (in Ref. [10], simulations were performed for desorption energies of $1200 \, \text{J mol}^{-1}$, $1400 \, \text{J mol}^{-1}$, and $1600 \, \text{J mol}^{-1}$).

In summary, the cold trap characterization measurements support the simulation results in Ref. [10] that the reduction factor of the CPS is well above 8 orders of magnitude. For a desorption energy of $1600 \, \text{J mol}^{-1}$, the simulated reduction factor decreases by three orders of magnitude to 10^{12} if the desorption of tritium molecules due to radioactive decays of adsorbed tritium is included. Therefore, this process will be the dominant cause of desorption compared to the thermal desorption for a desorption energy of $1553 \, \text{J mol}^{-1}$ in the case of tritium operation [10]. Nevertheless, the CPS reduction factor in standard KATRIN operation still exceeds the requirement of 10^7 by several orders of magnitude.

6. Summary

The cryogenic pumping section of the KATRIN experiment has to reduce the incoming neutral tritium flow by at least seven orders of magnitude in order to prevent a significant increase in background rate in the KATRIN spectrometers. This is achieved with an argon frost layer, prepared on a gold plated beam tube cooled to about 3 K. During commissioning, a dedicated measurement setup was used, making it possible to inject deuterium with a controlled injection rate. The results of two measurements, a longterm measurement at nominal configuration and a temperature dependent measurement of the cold trap, showed that the requirement is met and even surpassed by at least one order of magnitude. Repeating these measurements with tritium is not feasible since the required tritium flow would contaminate the spectrometer section. Therefore, the application of the measured results for tritium operation relies on simulations described in [10]. These results allowed a safe operation with tritium at the first KATRIN tritium measurement campaign in 2019 and the years to follow.

CRediT authorship contribution statement

C. Röttele: Writing – review & editing, Writing – original draft, Visualization, Validation, Supervision, Software, Methodology, Investigation, Formal analysis, Data curation, Conceptualization. **M. Steidl:** Writing – review & editing, Supervision, Project administration, Investigation, Conceptualization. **M. Sturm:** Writing – review & editing, Resources, Conceptualization. **M. Röllig:** Writing – review & editing, Resources, Investigation, Conceptualization. **A. Marsteller:** Writing – review & editing, Resources. **L. Schimpf:** Writing – review & editing, Software. **F. Friedel:** Writing – review & editing, Methodology, Conceptualization. **A. Jansen:** Writing – review & editing, Resources. **W. Gil:** Writing – review & editing, Resources, Investigation. **M. Schrank:** Writing – review & editing, Resources. **J. Wolf:** Writing – review & editing, Validation, Methodology. **G. Drexlin:** Writing – review & editing, Supervision, Project administration, Funding acquisition. **B. Bornschein:** Writing – review & editing, Supervision, Project administration.

Declaration of competing interest

The authors declare that they have no known competing financial interests or personal relationships that could have appeared to influence the work reported in this paper.

Data availability

Data will be made available on request.

Acknowledgments

References

[1] KATRIN collaboration, KATRIN Design Report, FZKA scientific report 7090, 2005, URL https://publikationen.bibliothek.kit.edu/270060419.

[2] M. Aker, K. Altenmüller, M. Arenz, et al., Improved upper limit on the neutrino mass from a direct kinematic method by KATRIN, Phys. Rev. Lett. 123 (22) (2019) http://dx.doi.org/10.1103/physrevlett.123.221802.

[3] A. Picard, H. Backe, H. Barth, et al., A solenoid retarding spectrometer with high resolution and transmission for keV electrons, Nucl. Instrum. Methods Phys. Res. B 63 (3) (1992) 345–358, http://dx.doi.org/10.1016/0168-583X(92)95119-C.

[4] S. Mertens, G. Drexlin, F. Fränkle, et al., Background due to stored electrons following nuclear decays in the KATRIN spectrometers and its impact on the neutrino mass sensitivity, Astropart. Phys. 41 (2013) 52–62, http://dx.doi.org/10.1016/j.astropartphys.2012.10.005.

[5] F. Priester, M. Sturm, B. Bornschein, Commissioning and detailed results of KATRIN inner loop tritium processing system at tritium laboratory karlsruhe, Vacuum 116 (2015) 42–47, http://dx.doi.org/10.1016/j.vacuum.2015.02.030.

[6] O.B. Malyshev, C. Day, X. Luo, F. Sharipov, Tritium gas flow dynamics through the source and transport system of the karlsruhe tritium neutrino experiment, J. Vac. Sci. Technol. A 27 (1) (2009) 73–81, http://dx.doi.org/10.1116/1.3039679.

[7] L. Kuckert, F. Heizmann, G. Drexlin, F. Glück, M. Hötzel, M. Kleesiek, F. Sharipov, K. Valerius, Modelling of gas dynamical properties of the katrin tritium source and implications for the neutrino mass measurement, Vacuum 158 (2018) 195–205, http://dx.doi.org/10.1016/j.vacuum.2018.09.036.

[8] A. Marsteller, B. Bornschein, L. Bornschein, et al., Neutral tritium gas reduction in the KATRIN differential pumping sections, Vacuum 184 (2021) 109979, http://dx.doi.org/10.1016/j.vacuum.2020.109979.

[9] O.B. Malyshev, Tritium migration along the cryopumping section, J. Vac. Sci. Technol. A: Vac. Surfaces Films 26 (1) (2008) 68, http://dx.doi.org/10.1116/1.2816945.

[10] F. Friedel, C. Röttele, L. Schimpf, et al., Time-dependent simulation of the flow reduction of D_2 and T_2 in the KATRIN experiment, Vacuum 159 (2019) 161–172, http://dx.doi.org/10.1016/j.vacuum.2018.10.002.

[11] M. Aker, K. Altenmüller, J.F. Amsbaugh, et al., The design, construction, and commissioning of the KATRIN experiment, 2021, arXiv:2103.04755.

[12] W. Gil, J. Bonn, B. Bornschein, et al., The cryogenic pumping section of the KATRIN experiment, IEEE Trans. Appl. Supercond. 20 (3) (2010) 316–319, http://dx.doi.org/10.1109/TASC.2009.2038581.

[13] A. Beglarian, E. Ellinger, N. Haußmann, et al., Forward beam monitor for the KATRIN experiment, 2021, arXiv:2101.11495.

[14] M. Arenz, W.-J. Baek, M. Beck, et al., First transmission of electrons and ions through the KATRIN beamline, J. Instrum. 13 (04) (2018) P04020, http://dx.doi.org/10.1088/1748-0221/13/04/p04020.

[15] S.A. Nepijko, I. Rabin, W. Schulze, Morphology of frozen rare-gas layers, ChemPhysChem 6 (2) (2005) 235–238, http://dx.doi.org/10.1002/cphc.200400420.

[16] C. Röttele, Tritium suppression factor of the KATRIN transport section (Ph.D. thesis), Karlsruher Institut für Technologie (KIT), 2019, http://dx.doi.org/10.5445/IR/1000096733.

[17] R. Kersevan, M. Ady, Recent developments of Monte-Carlo codes Molflow+ and synrad+, in: Proc. 10th International Particle Accelerator Conference (IPAC'19), Melbourne, Australia, 19-24 May 2019, in: International Particle Accelerator Conference, (10) JACoW Publishing, Geneva, Switzerland, 2019, pp. 1327–1330, http://dx.doi.org/10.18429/JACoW-IPAC2019-TUPMP037.

[18] MKS Instruments Inc., HPS products series 423 I-MAG cold cathode ionization vacuum sensor, 2009.